Targeting Control of Chaotic Systems

Erik M. Bollt

Department of Mathematics and Computer Science
Clarkson University, Potsdam, NY 13699, USA
bolltem@clarkson.edu

Abstract. Targeting control of chaos is concerned with taking advantage of sensitive dependence to initial conditions to coax a dynamical system to following a desirable trajectory. In other words, it is taking advantage of the butterfly effect so that the rich spectrum of possible trajectories embedded within a chaotic attractor can be selected with extremely small energy input. We review historical and popular approaches which fall under this general area in an attempt to reveal these techniques in a useful manner for applied scientists.

1 Introduction: Is "Controlling Chaos" an Oxymoron?

Over many years, chaos has been shown to be an interesting and even common phenomenon in nature. Chaotic systems are characterized by two defining properties: 1) *Sensitive Dependence* to Initial Conditions, 2) *Transitivity*[1] [25, 26]. Chaos has been shown to exist in a wide variety of settings: in fluid dynamics such as Raleigh-Bernard convection, in chemistry such as the Belousov-Zhaobitinsky reaction, in nonlinear optics in certain lasers, in celestial mechanics, in electronics such as Chua's circuit, in the flutter of an overdriven airplane wing, some models of population dynamics, and likely in meteorology, physiological oscillations such as certain heart rhythms as well as brain patterns. A complete list of natural systems which can potentially become chaotic would be too large to publish here. Nonetheless, chaos was not considered a desirable property in engineering control practice.

In 1990, Ott, Grebogi, and Yorke [2] (OGY) published a paper which most importantly, to this discussion, served as a case study which dispelled the paradigm that chaos is undesirable. The answer to, "Why Chaos," is this: in [2], the authors showed that any unstable periodic orbit of the system can be stabilized with small energy feedback control, and since a chaotic attractor is expected to be dense with periodic orbits, there is an arbitrarily rich array of different dynamic behaviors to choose amongst, already built into such a system, all accessible via small energy inputs.

The OGY technique essentially stabilizes an unstable periodic orbit by a specialized version of the pole-placement technique [3] applied to the linearized system, when trajectories have already tracked closed to the to-be

[1] Transitivity is equivalent to the statement that there exists a dense orbit.

stabilized orbit. Ergodicity is relied upon to ensure that such close encounters will occur. Since waiting times to apply the feedback control can be very long,[2] the next obvious question is how does one shorten the waiting time. This leads to the targeting problem. In a sense, the OGY solution to the targeting problem is ergodicity plus time.

The initial surprise with the oxymoron of the phrase "controlling chaos" comes from the fact that while a chaotic system is impossible to predict in the long run, it still arises in a deterministic system, which is therefore predictable in the short run. The short term evolution is deterministic, predictable, and controllable. In Fig. 1, we see the evolution of two initially very close initial conditions. At first their evolutions are close and predictable, a consequence of the usual Lipschitz continuity result that output of such a differential equation is continuous with respect to initial conditions [4]. In the long run, we see that the two trajectories are quite different; this is the numerical experiment that lead E. Lorenz to the historically important observed problem of sensitive dependence to initial conditions when predicting the weather. Now, considering the exponential growth rate of such errors from an optimistic standpoint, a vanishingly small energy input has the potential to yield a wide range of outcomes. The problem of programming when and how much those perturbations should be applied is the targeting problem.

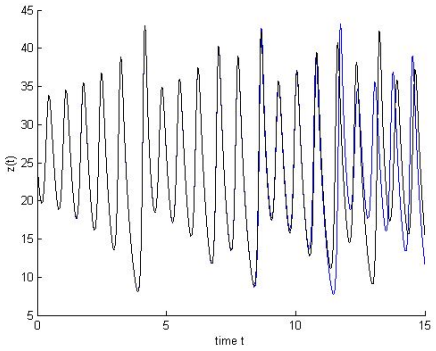

Fig. 1. Sensitive dependence to initial conditions in the famous Lorenz equations [1], $\dot{x} = 10(y - x), \dot{y} = x(28 - z) - y, \dot{z} = xy - (8/3)z$. Shown is the evolution of the z-time series from two nearby initial conditions.

2 Statement of the Targeting Problem

We formulate the targeting problem in terms of a discrete-time system. Let,

$$\mathbf{z}_{n+1} = \mathbf{f}_\lambda(\mathbf{z}_n), \tag{1}$$

[2] See [2,3] for explicit formulation of the scaling of expected wait time as a function of perturbation energy, for the map formulation of the problem

where $\mathbf{z} \in \Re^m$ is the phase-space variable, and $\lambda \in \Re^p$ are adjustable control variables. Later in the chapter, we will discuss continuous-time systems in terms of Poincaré section, to generalize the following techniques.

Suppose at time zero the initial state $\mathbf{z}_0 = \mathbf{a}$, but we wish to bring the system to (near) $\mathbf{z}_i \approx \mathbf{b}$ as "quickly" as possible, and subject to small energy input. The point $\mathbf{b}$ may for example be one iterate of a periodic orbit.

We have shown [29] that a general formulation of the targeting problem that can then be adapted for stabilization by feedback control in a differential equation is to find a "good" ϵ-chain orbit. See Fig. 12.

- **Define** an ϵ-*chain* from $\mathbf{a}$ to $\mathbf{b}$ as a set of points $\{\mathbf{z}_i\}_{i=0}^m$ such that,

$$\mathbf{z}_{i+1} = \mathbf{f}_\lambda(\mathbf{z}_i) + \epsilon_i, \tag{2}$$

where

$$|\epsilon_i| < \epsilon, \tag{3}$$

are the sequence of (small) errors, $\mathbf{z}_0 = \mathbf{a}$, and $\mathbf{z}_m \in N_\epsilon(\mathbf{b})$.

Here the notation $N_\epsilon(\mathbf{b}) = \{\mathbf{y} : |\mathbf{b} - \mathbf{y}| < \epsilon\}$ denotes an ϵ-neighborhood of $\mathbf{b}$.

The reason for this formulation is that an ϵ-chain can be stabilized as a sequence of two-point boundary value problems which are expected to be computably solvable when ϵ is small; see Chapter 5 for more discussion on this point. Whereas, the full two-point boundary value problem of a fast-transporting true orbit ($\epsilon = 0$) would be hard for long time, we will effectively break the problem into a sequence of short and easy such problems.

Note that without an objective function to qualify the word "good", we might choose any transporting orbit. The transitivity part of the definition of chaos implies infinitely many n such that $\mathbf{a} \in \mathbf{f}^{-n}(N_\epsilon(\mathbf{b}))$, but n is usually large if ϵ is small.

Objective: fast and small energy A reasonable objective function should balance short time, with low energy. Omitting either yields trivial extremes: if $\epsilon \sim O(1)$ then one can hit any target in one step, while if short time is not required then we generally need to do nothing since the orbit of $\mathbf{a}$ will wander near $\mathbf{b}$ *eventually* and indeed that is the original OGY solution to targeting [2].

We state our favorite objective functions:

- Minimum iterate, constrained energy,

$$F(\{\mathbf{z}_i\}_{i=0}^m) = m, \tag{4}$$

subject to $\{\mathbf{z}_i\}_{i=0}^m$ is an ϵ-chain such that $\epsilon < \epsilon_{max}$.

Other reasonable cost functions [5] might be continuous time, which will be different in general than number of iterates when time-of-flight between Poincaré surfaces is nonuniform, or perhaps fuel required in designing a space flight mission design, or reaction rate in a chemical reaction for example.

As far as we know, solving any such problem as an optimal control problem is in general an open problem. Nonetheless, it is important to have a good objective function to have a basis to compare quality between various candidate solutions. Surprisingly, there is still almost no mention of objective or cost in the now relatively large literature on targeting.

3 Targeting: A Simple and Instructive One-Dimensional Example

We present here a concrete example of targeting, which while limited in scope in that it only works for one-dimensional maps, it serves as a "cartoon" of how sensitive dependence can be leveraged and useful. The following was inspired by [6, 7], but was explicitly developed in [8] as a undergraduate student project.

Consider the logistic map,

$$x_{n+1} = f_r(x_n) = rx_n(1 - x_n), \tag{5}$$

and given the initial condition $a = x_0 = 0.4$ for example, suppose we wish to hit the target $b = 0.8$ in as few iterates as possible subject to small parameter variations. Let $r_0 = 3.9$ be the nominal parameter value, and constrain,

$$3.8 \leq r_0 + \delta r \leq 4.0, \tag{6}$$

for the example.

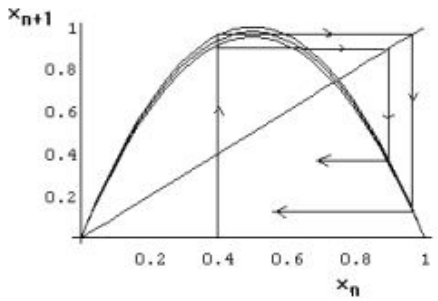

Fig. 2. Parametric variations in the logistic map yields an initially small interval of possible outcomes, which then grows exponentially under sensitive dependence to initial conditions.

Iterating the initial condition under the entire family of maps, corresponding to the parameter interval, we get (See Fig. 2),

$$x_1 \in f_{[3.8,4.0]}(0.4) = [0.91, 0.96]. \tag{7}$$

Then returning the parameter to $r = r_0$, for simplicity of the example, we get,

$$\begin{aligned} x_2 &\in f_{3.9}([0.91, 0.96]) = [0.14976, 0.312998], \\ x_3 &\in f_{3.9}([0.14976, 0.312998]) = [0.496595, 0.838618]. \end{aligned} \tag{8}$$

At this point we see that the target is bracketed, and since f_r is continuous with respect to r, the intermediate value theorem implies a root of the equation,

$$f_{3.9} \circ f_{3.9} \circ f_r(0.4) = 0.8, \tag{9}$$

for the unknown control parameter r. Bisection yields, $r = 3.831890....$

The lesson we learn from this example is that a small and *deliberate* perturbation quickly grows to fill the compact phase space, and hence sensitive dependence to initial conditions can be helpful to design a responsive control system.

In fact, this simple technique can be adapted to experimental systems [9, 10]. However, the specific details of this algorithm requires a one-dimensional map. One-dimensional maps are however surprisingly common in nature, since strong dissipation often creates surprisingly low-dimensional attractors. For example, plotting successive maxima of the $z(t)$ time-series seen in Fig. 1 of the Lorenz system is known [1] to yield a one-humped map.

3.1 The higher-dimensional generalization

The direct generalization of the above algorithm is to iterate a neighborhood $N_\epsilon(\mathbf{a})$ forwards under f, and perhaps iterate $N_\epsilon(\mathbf{b})$ backwards under f^{-1} if the inverse exists. This is the idea behind the work by Shinbrot, Ott, Grebogi and Yorke, [11] sometimes called SOGY. The idea is to resolve (the boundary of) $N_\epsilon(\mathbf{a})$ and $N_\epsilon(\mathbf{b})$ into a fine enough grid so that iterating under f and f^{-1} if it exists allows us to solve for an m and n which solve,

$$f^m(N_\epsilon(\mathbf{a})) \cap f^{-n}(N_\epsilon(\mathbf{b})) \neq \emptyset, \tag{10}$$

Deciding the intersection of two regions defined by grid points on their boundaries reduces to a problem of computational geometry: deciding crossings of pairs of vectors from successive grid points of from each boundary. One simple solution in terms of the cross product can be found in, [12].

This method works adequately well when there exist a small $p = m + n$ solution of Eq. (10). Simple low-dimensional attractors, such as the Henon

attractor lend themselves well to this technique, [11, 12]. However, if the minimal solution $p = m+n$ to Eq. (10) is not small, then the problem becomes computationally impossible. Since a grid of r points, spread uniformly around $N_\epsilon(\mathbf{a})$, is expect to spread approximately by factors of λ_u, where $\lambda_u > 1$ is the largest Lyapunov number, then those points which were initially $2\pi\epsilon/r$ apart are expected to be approximately $2\pi\epsilon/r\lambda_u^m$ apart for large m. Quickly, no initial grid is fine enough that $2\pi\epsilon/r\lambda_u^m$ is still small for large m. Likewise, if $\lambda_s < 1$ is the smallest Lyapunov number, the s initial points around $N_\epsilon(\mathbf{b})$ gets spread too thinly according to, $2\pi\epsilon/s\lambda_u^{-n}$. Leaving the simple details to those interested, it is clear that sensitive dependence works against us here: it is computationally impossible to resolve intersections such as those depicted in Fig. 3 for large p by the brute force of iterating grids.

Specifically, transport is too slow to directly solve Eq. (10) in many systems, such as for example, in higher dimensions [16], or in Hamiltonian systems with resonance layers, [12–15].

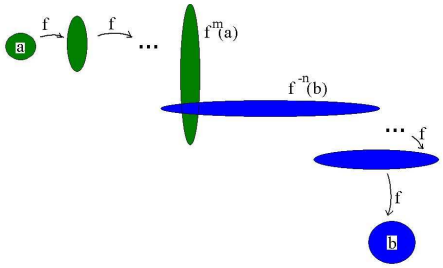

Fig. 3. The SOGY [11] is a constructive targeting method. A forward iterate of a neighborhood of a which is found to intersect an inverse iteration of a neighborhood b implies, by continuity, existence of fast trajectory. The difficulty is that representing $N_\epsilon(\mathbf{a})$ and $N_\epsilon(\mathbf{b})$ with a fine enough grid so that $f^m(N_\epsilon(\mathbf{a}))$ and $f^{-n}(N_\epsilon(\mathbf{b}))$ can still be resolved accurately enough at time of intersection, for large $p = m + n$ is exponentially memory consuming.

3.2 A web approach to higher-dimensional targeting

The exponential growth of $N_\epsilon(\mathbf{a})$ upon iteration is equivalent to growth of possibilities of outcomes, and this idea is essentially related to the entropy of the system. The first technique to address growth of possibilities used a tree structure as designed by E. Kostelich *et. al.*, [16]. See also, [17, 18].

The idea of the Kostelich technique is to find a tree of paths leading to a target point b. For example, if a free-running trajectory leads to $N_\epsilon(\mathbf{b})$ in say 30 iterates, then keep that last 30 iterates, and call them the primary trunk of the tree and label them $\{\mathbf{z}_i^1\}_{i=1}^{30}$. Then continuing to iterate, one

expects a recurrence to one of the points $\{\mathbf{z}_i^1\}_{i=1}^{30}$. Record those, say 30, previous iterates and call them, $\{\mathbf{z}_i^{2,1}\}_{i=1}^{30}$, and these are a primary branch. By construction, $\mathbf{z}_{30}^{2,1} \in N_\epsilon(\mathbf{z}_i^1)$ for some i. Likewise collect several ($j = 1, 2..$) more primary branches, by simple iteration, and collecting primary trunk intersections, $\{\mathbf{z}_i^{2,j}\}_{i=1}^{30}$. Similarly by recurrence and iteration construct secondary branches of paths which lead to primary branches, etc. See Fig. 4. When we are done, we have constructed a tree of paths, which hopefully covers a significant measure of the attractor, and more specifically every possible initial condition is no more than a few iterates from one of the members of the tree. In [16], the authors showed this technique to be successful in the four-dimensional double-rotor map [19].

In a sense, this technique is a generalization of the OGY technique. In the OGY technique, there is an essentially random transient time while one waits for the orbit to wander into the capture window around a periodic orbit. With the Kostelich tree, one also has a transient time of waiting while the orbit wanders into a now extended set of neighborhoods of point, and active feedback control is launched as soon as any one of those pre-recorded points is approached.

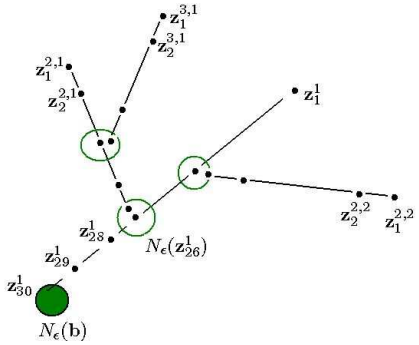

Fig. 4. Caricature of a typical tree of ϵ-chain paths leading to a target point $\mathbf{b}$, as in [16].

3.3 Targeting through recurrence through resonance layers and to the moon

Uncontrolled transport in one and a half degree of freedom Hamiltonian systems with resonance layers is particularly slow, [20, 21] and the above described techniques do not work well, [12–15]. Consider for example the Chirikov Standard map,

$$\mathbf{z}' = \begin{pmatrix} y' \\ x' \end{pmatrix} = T(\mathbf{z}) \equiv \begin{pmatrix} y - \frac{k}{2\pi}\sin(2\pi k x) \\ y - \frac{k}{2\pi}\sin(2\pi k x) + x \end{pmatrix}, \tag{11}$$

often used as the prototypical example of an area-preserving twist map. Specifically, we expect KAM circles which become "cantori" as k increases, but which still serve as partial barriers inhibiting transport. This is responsible for the sticky islands-around-islands effect. Chaotic transport mechanisms provides that a fast orbit must pass through the "turnstiles" [21] via "lobe dynamics" [66] corresponding to intermediate barriers. It follows that a fast orbit should pass through these localized regions exactly once [12, 14]. The constructive approach is to compute the turnstiles, and perhaps find short orbit segments between them, such as was tried in [12, 14] and also [27], but a problem with this approach is the fact that there are infinitely many resonances which layer the phase space with a great deal of resonance overlap, and it is not obvious which are most important. We have found the explicit approach to be unnecessary by the following technique which provides that a slow orbit goes through all of the intermediate obstacles and more, and thus signals the fast way, needing only some shortening.

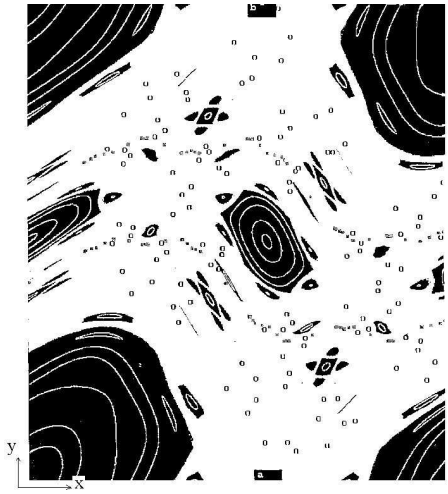

Fig. 5. A fast orbit of the standard map, (the "o"'s) from near $\mathbf{a} = (x_a, y_a) = (0.5, 0.0)$, to near $\mathbf{b} = (x_b, y_b) = (0.5, 1.0)$. Here, $k = 1.25 > k_c$, and a slow test orbit wanders in the "chaotic sea" (the large white region) from near $\mathbf{a} =$ to near $\mathbf{b}$. The test orbit which may wander near the remaining resonance islands remains for a long sojourn before again escaping to continue towards the target. A 80307 test orbit has been used to find a nearby 131 fast orbit.

As a concrete example, we investigate transport from a neighborhood of the $(0, 1)$ hyperbolic point to a neighborhood of the $(1, 1)$ resonance. The notation (p, q) denotes the frequency of an orbit, i.e. q iterations of the map results in exactly p wraps around the cylinder: $T^q(\mathbf{z}) = \mathbf{z} + p$. The starting

point $(0,1)$ **a** is located at $(x_a, y_a) = (0.5, 0.0)$, and (1,1), our target point **b**, at $(x_b, y_b) = (0.5, 1.0)$.

Such an orbit does not exist if $k < k_c \approx 0.97163540631...$ [21]; k_c is the parameter value at which the last invariant curve dividing phase space between $(0,1)$ and $(1,1)$ becomes a cantorus. The most robust curves between $(0,1)$ and $(1,1)$ are the circles with rotation frequencies $\frac{1}{\gamma}$ and $\frac{1}{\gamma^2}$, where $\gamma = \frac{1+\sqrt{5}}{2}$ is the golden mean. If $k > k_c$, there are no invariant curves separating vertical transport of the cylinder, and therefore according to Mather's theorem [22], there exists a heteroclinic connection between the $(0,1)$ and $(1,1)$ orbits for which we will search.

For $k > k_c$, the golden mean invariant curves become cantori. They have the smallest lobe areas, and hence, represent the most difficult barriers to transport. An arbitrary orbit will typically pass through these lobes many times before finally reaching the target point **b**. This effect also occurs when an orbit is trapped near an island, and near islands around islands, and so on. This phenomenon has been successfully modelled using Markov trees [23,24]. It was found that a point initially "near" a KAM surface has a survival probability $F(t)$ is asymptotic to $t^{-\alpha}$ and that the orbit will still be near the surface at large time t with small constant α [24]. Therefore in the presence of KAM surfaces, we find long correlations and, hence, roughly power law decay. However the important point is that, without knowing where the lobes are located, recurrence is a way of locally detecting globally inefficient orbits.

The idea of cutting recurrent loops is as follows:

- All orbits go through intermediate barriers, which for area preserving maps are the turnstiles. Distinguishing fast from slow is that fast transporting orbits go through necessary pseudo-barriers (turnstiles) exactly once, and do not go through unnecessary barriers (drawing closer to islands) at all. Slow transporting orbits go through necessary pseudo-barriers (turnstiles) some odd number of times greater than once, and go through turnstiles leading to islands some even number of times. See caricature in Fig. 6.
- Unnecessary or slowing transport is signaled by recurrence in the turnstiles.
- A slow transporting orbit may be used as a test orbit, and the long recurrent loops can be removed if the error can be forced to be small by the hyperbolicity method described below in Eq. (12). We define a recurrence as unnecessary when a solution to Eq. (12) is found.

Once a recurrence has been identified between $\mathbf{z}_i$ and $\mathbf{z}_{i+s}$, to find an ϵ-chain which skips the s-step recurrent loop, we must solve the following two-point boundary valued problem. See Fig. 7. We require that a point on the unstable direction f_u at $\mathbf{z}_{i-m}$ lands on the stable direction f_s at $\mathbf{z}_{i+s+m}$. Thus we must find ξ which solves [15],

$$[T^{2m}(\mathbf{z}_{i-m} + \xi f_u) - \mathbf{z}_{i+s+m}] \times f_s = 0. \tag{12}$$

To find the stable and unstable foliations [14, 67], recall that the Jacobian matrix rotates a vector in the tangent space towards the unstable direction, and the Jacobian matrix of the inverse map T^{-1} rotates a vector towards the stable direction (if they exist!). Therefore, in practice, we choose an arbitrary unit vector $\mathbf{u}$ and forward multiply, starting at $\mathbf{z}_{-n}$, the Jacobian matrices along the orbit to $\mathbf{z}$, normalizing the vector at each step:

$$DT^n|_{z_{-n}} \cdot \mathbf{u} \equiv DT|_{z_{-1}} \cdot DT|_{z_{-2}} \cdot ... \cdot DT|_{z_{-n}} \cdot \mathbf{u} \to f_u(\mathbf{z}) \text{ as } n \to \infty. \quad (13)$$

Likewise, the stable direction is formed from the inverse Jacobian starting at $T^n(\mathbf{z})$.

$$DT^{-n}|_{z_n} \cdot \mathbf{u} \equiv DT^{-1}|_{z_1} \cdot DT^{-1}|_{z_2} \cdot ... \cdot DT^{-1}|_{z_n} \cdot \mathbf{u} \to f_s(\mathbf{z}) \text{ as } n \to \infty. \quad (14)$$

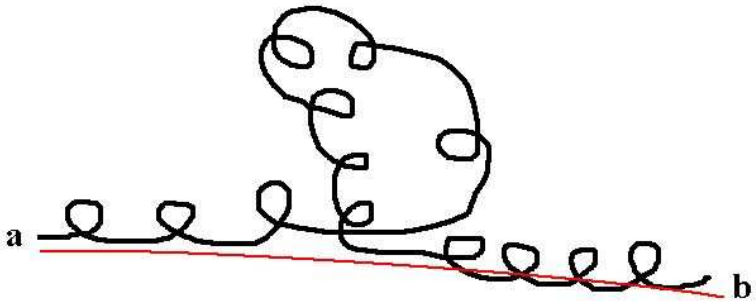

Fig. 6. Caricature of a slow transporting orbit, which recurs with itself many times during its flight to **b**. The fast orbit in red does not suffer unnecessary recurrence.

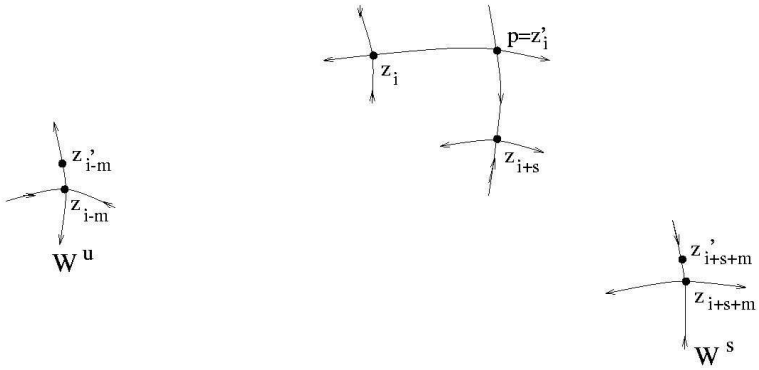

Fig. 7. Hyperbolicity is used to diminish a recurrence error, and to remove the recurrent loop.

Considering the specific standard map $k = 1.25$, with $\mathbf{a}$ and $\mathbf{b}$ shown in Fig. 5. The first recurrence that we can successfully remove from one representative 80307 step orbit is between $\mathbf{z}_{16}$ and $\mathbf{z}_{78704}$ which recurs to a distance of $\delta = 0.08$. In this example, we construct an orbit patch $\{\mathbf{z}'_1, ..., \mathbf{z}'_{31}\}$ such that the error to perturb on to the orbit patch is only $\|\mathbf{z}'_1 - \mathbf{z}_1\| = 0.002$, and the error to perturb back off of the orbit patch is $\|\mathbf{z}'_{31} - \mathbf{z}_{78720}\| = 0.002$. With this single patch, we have already demonstrated a 1619 step epsilon chain orbit near our original orbit. By finding every recurrence within a threshold $\delta = 0.1$ and cutting those that can be patched within the error $\epsilon = 0.005$ we eventually construct a 131 step epsilon chain orbit including 13 overlapping patches. The largest error found in this example was $\|T(\mathbf{z}_{92}) - \mathbf{z}_{93}\| = 0.003$, but there were several others of the same order.

As an example of the utility of targeting in area-preserving maps, consider the circular, Restricted-Three-Body Problem (RTBP), defined by the Hamiltonian [28],

$$H = \frac{(p_x + y)^2 + (p_y - x)^2 + p_z^2}{2} - \Omega(x, y, z), \tag{15}$$

where,

$$\Omega(x, y, z) = \frac{x^2 + y^2}{2} + \frac{1 - \mu}{r_1} + \frac{\mu}{r_2} + \frac{\mu(1 - \mu)}{2}, \tag{16}$$

and,

$$r_1 = \sqrt{(x + \mu)^2 + y^2 + z^2}, r_2 = \sqrt{(x - 1 + \mu)^2 + y^2 + z^2}. \tag{17}$$

The resulting equations of motion,

$$\begin{aligned} \dot{x} &= \frac{\partial H}{\partial p_x} = p_x + y, \ \dot{p_x} = -\frac{\partial H}{\partial x} = p_y - x + \Omega_x, \\ \dot{y} &= \frac{\partial H}{\partial p_y} = p_y - x, \ \dot{p_y} = -\frac{\partial H}{\partial y} = -p_x - y + \Omega_y. \end{aligned} \tag{18}$$

evolve as a flow in $\Re^4$, but there is the Jacobi integral, which is constant along the flow,

$$J(x, y, z, \dot{x}, \dot{y}, \dot{z}) = (\dot{x}^2 + \dot{y}^2 + \dot{z}^2) - 2\Omega(x, y, z), \tag{19}$$

whose existence implies that the flow occupies a 3-dimensional submanifold. Thus a Poincaré mapping, of x versus $\dot{x}$ for each point when the flow transverse $y = 0$ with $\dot{y} > 0$ yields an area preserving map. See Fig. 8.

The RTBP is considered a good initial model of the Earth-Moon system, in which a third small particle, such as a spaceship is too small to essentially alter the integrable Kepler motion of the primaries. Choosing realistic relative masses, $m_1/m_2 = 0.0123$, there is insufficient energy in the system for an Earth-Moon escape for Jacobi-integral $J < -3.1883$. We choose

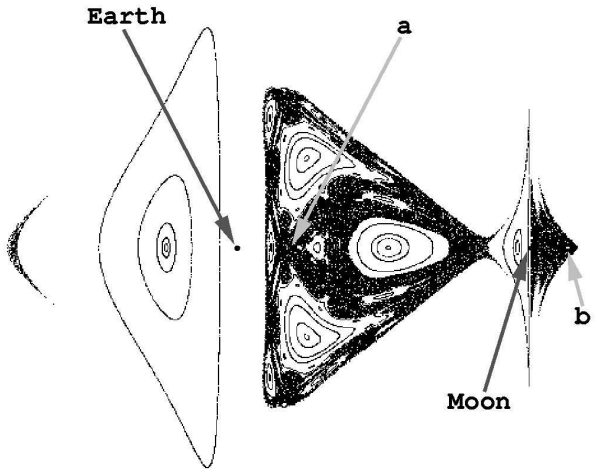

Fig. 8. Circular Restricted-Three Body Problem, as the Poincaré mapping, $(x, \dot{x})$ for each transverse point when $y = 0$ with $\dot{y} > 0$.

$J = -3.17948$, just after transport is possible, and well below the $J = -2.761$ energy required for the pictured Hohmann transfer. Our technique reduced a "Chaotic test orbit" (See Fig. 8) from 10710 iterates to 58 iterates on Poincaré section, or down to 2.05 years. Whereas the Hohmann transfer (Apollo-type mission) shown takes 6.61 days and a $1219.8m/s$ impulse budget, the chaotic transfer requires 2.05 years and only $749.6m/s$ of impulse, most of it to boost from the same circular orbit around the Earth to the $J = -3.17948$ transferring parameter. Since rockets expel most of their weight as ejected fuel, this translates to 83% more payload with a constant sized booster. Thus the theme of targeting in chaos: *we can trade time for energy.*

4 Combinatorial Targeting and Symbolic Dynamics

The tree description of the growing possible orbits, such as that depicted in Fig. 4 is suggestive of the combinatorial explosion in possible outcomes, which is essentially a discrete approximation of the notion of sensitive dependence to initial conditions. In [5, 29], we posed the targeting control problem in terms of approximating the action of a dynamical system on its phase space as a directed graph between vertices which label a rectangular covering of the phase space. In fact, a map on a topology of open sets can be considered as a directed graph between the sigma algebra of open sets; such an abstract description is simplified by a generating partition, from which follows the symbolic dynamics [30–32]. We and others have shown that combinatorial [5, 29, 33] and symbolic methods [10, 34–37], and [56] are a complete and efficient descriptions of all possible orbits of a dynamical system. Within

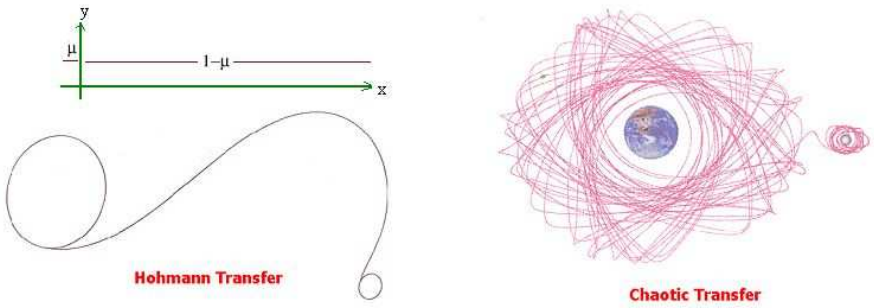

Fig. 9. Left: A "Hohmann transfer" in the Circular Restricted-Three Body Problem; this is essentially skeet shooting in a $1/r^2$ potential well and it is the sort of trajectory the Apollo astronauts flew. Right: A chaotic transfer. The Homann transfer takes less time but substantially more fuel than the chaotic transfer.

such a description, targeting is reduced to the simpler and well-understood discrete problem of path searching in graph theory. For example, the shortest path through an unweighted directed graph is found by the breadth-first-search algorithm and through a positively weighted graph by the Dijkstra algorithm [38, 39].

For these reasons, we will briefly review the role of symbolic dynamics in dynamical systems, first for one-dimensional mappings, followed by diffeomorphisms of the plane. Then following, we review application of symbolic dynamics to targeting control.

4.1 One-dimensional maps with a single critical point

First consider a one-humped interval map, such as the logistic map Eq. (5) or Lorenz's successive maxima map, which follows by plotting just the local maxima of the $z(t)$ time-series from the Lorenz differential equations [1] in Fig. 1 and similarly for many other systems.

$$f : [a, b] \to [a, b]. \tag{20}$$

Such a map "has" symbolic dynamics [40, 41] relative to a partition at the critical point x_c. Choosing a two symbol partition, labelled $\mathcal{I}$=$\{0, 1\}$, names iterates of an initial condition x_0 dynamically,

$$\sigma_i(x_0) = \begin{pmatrix} 0 \text{ if } f^i(x_0) < x_c \\ 1 \text{ if } f^i(x_0) > x_c \end{pmatrix}. \tag{21}$$

The function h labels each initial condition x_0 and corresponding orbit $\{x_0, x_1, x_2, ..\}$ by an infinite symbol sequence,

$$h(x_0) \equiv \sigma(x_0) = \sigma_0(x_0).\sigma_1(x_0)\sigma_2(x_0)... \tag{22}$$

Defining the "fullshift" $\Sigma_2 = \{\sigma = \sigma_0.\sigma_1\sigma_2... \text{ where } \sigma_0 = 0 \text{ or } 1\}$ to be the set of all possible infinite symbolic strings of $0's$ and $1's$, any given infinite symbolic sequence is a singleton (a point) in the fullshift space, $\sigma \in \Sigma_2$. The usual topology of open sets in the shift space Σ_2 follows the metric,

$$d_{\Sigma_2}(\sigma, \overline{\sigma}) = \sum_{i=0}^{\infty} \frac{|\sigma_i - \overline{\sigma}_i|}{2^i}, \tag{23}$$

which defines two symbol sequences to be close if they agree in the first several bits. Eq. (21) is a good "change of coordinates," or more precisely a homeomorphism,[3]

$$h : [a, b] - \cup_{i=0}^{\infty} f^{-i}(x_c) \to \Sigma_2', \tag{24}$$

under conditions on f, such as piecewise $|f'| > 1$.[4] The Bernoulli shift map moves the decimal point in Eq. (22) to the right, and "eliminates" the leading symbol,

$$s(\sigma_i) = \sigma_{i+1}. \tag{25}$$

All of those itineraries from the map f, Eq. (1) by Eq. (21), correspond to the Bernoulli shift map restricted to a subshift,[5] $s : \Sigma_2' \to \Sigma_2'$. Furthermore, the change of coordinates h is a conjugacy[6].

In summary, the previous paragraph simply says that corresponding to the orbit of each initial condition of the map Eq. (20), there is an infinite itinerary of $0's$ and $1's$, describing each iterate's position relative the partition in a natural way which acts like a change of coordinates such that the dynamical description is equivalent. For our purposes, controlling orbits of the map f in phase space which is an interval corresponds also to controlling itineraries in symbol space. The control over x composed with the change of coordinates h can essentially be considered to be a coding algorithm.

[3] A *homeomorphism* between two topological spaces A and B is a one-one and onto continuous function $h : A \to B$, which may be described loosely as topological equivalence.

[4] Note that pre-images of the critical point are removed from $[a, b]$ for the homeomorphism. This leaves a Cantor subset of the interval $[a, b]$. This is necessary since a shift space is also closed and perfect, whereas the real line is a continuum. This is an often over-looked technicality, which is actually similar to the well known problem when constructing the real line in the decimal system (the ten-shift Σ_{10}) which requires identifying repeating decimal expansions of repeating 9's such as for example $1/5 = 0.1\overline{99} \equiv 0.2$. The corresponding operation to the shift maps [25] is to identify the repeating binary expressions $\sigma_0.\sigma_1..\sigma_n0\overline{11} \equiv \sigma_0.\sigma_1..\sigma_n1\overline{11}$, thus "closing the holes" of the shift space Cantor set.

[5] A *subshift* Σ_2' is a closed and Bernoulli shift map invariant subset of the fullshift, $\Sigma_2' \subset \Sigma_2$.

[6] A *conjugacy* is a homeomorphism h between topological spaces A and B, which commutes maps on those two spaces, $\alpha : A \to A$, $\beta : B \to B$, then $h \circ \alpha = \beta \circ h$.

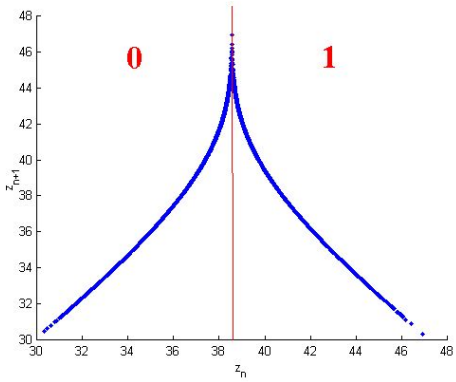

Fig. 10. Successive maxima map of the $z(t)$ variable, of the Lorenz flow $(x(t), y(t), z(t))$ from Fig. 1.

4.2 Higher-dimensional systems and symbolic dynamics of diffeomorphisms

Diffeomorphisms arise naturally by Poincaré mapping of a flow. In general, a diffeomorphism $f : M \to M$ is expected for an $N-1$ manifold M which is transverse to a flow in $\mathbf{R}^N$.

Symbolic dynamics of higher dimensional systems is still a highly active research area and details here are necessarily slight. In particular, we refer the reader to see [44–46]. The fundamental difference of dimensionality is that invertible maps and hence diffeomorphisms are necessarily simple in the interval, whereas in more than one dimension, there may be chaos. In the interval, only a many-to-one map allows for the folding property which is an ingredient of chaos. However, S. Smale [48] showed that the folding mechanism of a horseshoe allows for chaos in a planar diffeomorphism.

In the development in the previous subsections, the one-sided shifts reflect the noninvertible nature of the corresponding interval maps Eq. (1). The generalization of symbolic dynamics for invertible maps requires bi-infinite symbol sequences,

$$\Sigma_2 = \{\sigma = ...\sigma_{-2}\sigma_{-1}\sigma_0.\sigma_1\sigma_2... \text{ where } \sigma_0 = 0 \text{ or } 1\}. \tag{26}$$

The main technical difficulty of symbolic dynamics for a map with a more than one-dimensional domain is well defining a partition. A notion of Markov partitions is well defined[7] for Axiom A diffeomorphisms [49, 50], but

[7] R. Bowen [49,51], defined conditions for a partition of "rectangles" to be Markov. A topological partition $\{Q_i\}$ of open rectangles is Markov if, $\{Q_i\}$ have nonoverlapping interiors, such that when $f(Q_i) \cap Q_j \neq \emptyset$, then $f(Q_i)$ stretches across Q_j, in that stretching directions are mapped to stretching directions and contracting directions are mapped to contracting directions. Said more carefully, we require that $W^u(f_n(z), Q_i) \subset f_n(W^u(z, Q_i)$ and $f_n(W^s(z, Q_i) \subset W^s(f_n(z), Q_i)$.

such maps are not expected to be generic. The more general notion of a generating partition [30] is also well defined,[8] but particularly in the case of a nonuniformly hyperbolic dynamical system construction of the generating partition is an open problem for most maps. A well regarded conjecture for planar diffeomorphisms, such as the Henon map [44–46], is that the generating partition should be a curve that connects all "primary" homoclinic tangencies. See also [47, 52–55].

4.3 Learning the grammar in practice

In a physical experiment, corresponding to the one-dimensional map such as Eq. (1), it is possible to approximately deduce the grammar of the corresponding symbolic dynamics by systematic recording of the measured variables relative either to a reasonable approximation of the generating partition, or a fine grid. First note that any real measurement of an experiment consists of a necessarily finite data set. Therefore, in practice, it can be argued that there is no such thing as a grammar of infinite type in the laboratory. So without loss of generality, we may consider only grammars of finite type for our purposes. Such a subshift is a special case of a sophic shift [42, 43]. In other words, there exists a finite digraph which completely describes the grammar. All allowed words of the subshift, Σ' corresponding to itineraries of orbits of the map correspond to some walk through the graph.

For example, the Henon map,

$$(x_{n+1}, y_{n+1}) = f(x_n, y_n) = (1.8 - x_n^2 + by_n, x_n), \tag{27}$$

has a symbolic dynamics as represented in Fig. 11. For this picture, for the illustration, we have explicitly calculated the generating partition in terms of homoclinic tangencies discussed above, [44–47]. Iterates and pre-iterates of the critical curve finely partitions the phases space, but most importantly, it finely partitions the attractor. We see that since the attractor fails to cover all 2^4 labelled permutations of the 4-bit symbols, there are missing words, in this relatively coarse (for sake of artistic Caricature) approximation. In the directed graph approximation of the corresponding transitions on the

[8] Given a dynamical system $f : M \to M$, a *finite* collection of disjoint open sets, $\{B_k\}_{k=1}^K$, $B_k \cap B_j = \emptyset$ $(k \neq j)$, is defined to be a topological partition if the union of their closures exactly covers M: $M = \cup_{k=1}^K \overline{B_k}$, [Lind & Marcus, 1995]. The set of intersection of the images and pre-images of these elements $\cap_{i=-n}^n \mathbf{f}^{(-i)}(B_{\mathbf{x}_i})$ is in general open. For a faithful symbolic representation of the dynamics, the limit $\cap_{n=0}^\infty \cap_{i=-n}^n \mathbf{f}^{(-i)}(B_{\mathbf{x}_i})$ should be a single point if nonempty. Given a dynamical system $\mathbf{f} : \mathcal{M} \to \mathcal{M}$ on a measure space $(\mathcal{M}, F, \mu)$, a finite partition $P = \{B_k\}_{k=1}^K$ is generating if the union of all images and preimages of P gives the set of all μ-measurable sets F. In other words, the "natural" tree of partitions: $\vee_{i=-\infty}^\infty \mathbf{f}^i(P)$, always generates some sub-σ-algebra, but if it gives the full σ-algebra of all measurable sets F, then P is called *generating* [30]

attractor, observe that paths through the graph correspond to trajectories on the attractor, and cycles correspond to periodic orbits (or at least to ϵ-chain pseudo-orbits).

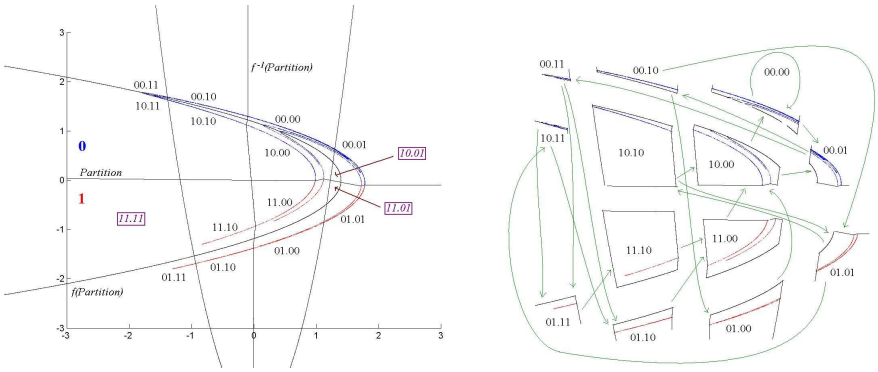

Fig. 11. Left, the Hénon attractor has a symbol dynamics generated by the w-shaped partition, which allows us to color the attractor Blue for current state is '0' above the curve, or Red for '1'. It is believed that iterates and pre-iterates of the curve generates the topology of opens sets. Right, using our coarse 4-bit approximation, we see all 4-bit transitions on the attractor, and hence all pseudo orbits are walks through the graph and cycles are pseudo-periodic orbits. This graph generates the symbolic dynamics Σ_2' on the attractor.

Forcing the symbolic dynamics, via forcing paths through the corresponding graphic descriptions is all that is necessary now to create ϵ-chain pseudo-orbits of the dynamical system. In the next section, we discuss making these into real orbits of a differential equations. We close by mentioning that we are actually controlling the information production of the dynamical system, which can either be viewed as a control strategy over orbits as we are interested here, or alternatively as a communication via chaos scheme as we [10, 34, 35] and others [36, 37] have researched extensively elsewhere. As a technical note of practical importance, we have found link-lists to be the most efficient method to record a directed graph together with its allowed transitions.

5 Forcing the Path: Feedback Control

We have seen in the previous section that combinatorial and symbolic description of trajectories are efficient for designing trajectories of the dynamical system as ϵ-chain pseudo-orbits. What remains to be discussed is how to force the orbit of a randomly chosen initial condition to follow the above designed pseudo-orbit "plans," in the case of a differential equation which is the necessary step to argue physical relevance of the above described techniques.

We will mention three main techniques: 1) Parametric feedback control which reduces to a sequence of two-point-boundary-valued-problems (TPBVP), 2) adaptive targeting, and 3) limiter control.

5.1 Parametric feedback control

By construction, the ϵ-chain pseudo-orbits are designed with small ϵ, and thus parametric control may be used [16, 29]. We refer the reader to Fig. 12 for what we hope is a clear pictorial description of this basic idea.

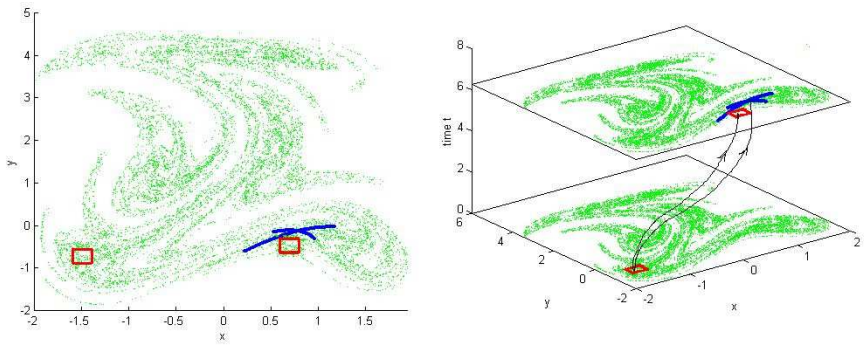

Fig. 12. Observed next responses due to parameter variations of the Duffing oscillator: $x'' + ax' + x^3 - x = b\sin(t)$, where $\lambda_0 = (a_0, b_0) = (0.02, 3)$. Left) Dots show $N = 10,000$ iterates of 2π-stroboscopic map. Bold squares show "from" and "to" nodes, in this (overly-large caricature) grid. Bold crossed curves show observed next responses due to maximal variations $|\delta\lambda| = (|\delta a|, |\delta b|) \leq (0.02, 0.25)$, where either δa or δb is varied separately, while the other is held fixed. Right) Caricature of flow between the piercings on the Poincaré section of the uncontrolled and controlled differential equation, and the target box.

Feedback control of a chaotic trajectory may be realized by small parameter variations. For example, given a flow of $\mathbf{z}(t) \in \mathbf{R}^N$ where we explicitly write the parameter dependence $\mathbf{p} \in \mathbf{R}^n$,

$$\dot{\mathbf{z}} = \mathbf{F}(\mathbf{z}, \mathbf{p}), \tag{28}$$

one can hope to effect the trajectory in a predictable manner in the short run. In particular, if the desired short-term response is small, a Lipschitz continuous right hand side F provides that small parameter variations should suffice. Furthermore for small enough desired short term responses, the required parameter variation can be usefully and easily found by directly solving the (TPBVP). More specifically, suppose that on surface of section M, the initial condition $\mathbf{z}_0 \in M$ flows forward under Eq. (28) to $\mathbf{z}_1 \in M$, $\mathbf{z}_1 = \mathbf{f}(\mathbf{z}_0) = \Phi_t(\mathbf{z}_0)$ (t is the time of flight of the mapping, which is generally not uniform with

respect to $\mathbf{z}$, and this is not a concern to us here) at next Poincaré surface piercing, under a nominal/uncontrolled parameter value $\mathbf{p}_0$. The Poincaré mapping we now denote,

$$\mathbf{f}(\mathbf{z}, \mathbf{p}) : M \to M, \tag{29}$$

to emphasize a family of mappings parameterized by adjustable parameter $\mathbf{p}$. If we prefer the next iterate to be $\mathbf{z}_{\text{desired}}$, then the next controlled response, is a solution to the equation,

$$\mathbf{z}_{\text{desired}} = \mathbf{f}(\mathbf{z}_0, \mathbf{p}_1) \tag{30}$$

whose solution is formally a TPBVP of the flow Eq. (28), where $\mathbf{p}_1$ is the unknown in the equation to be found, usually by shooting [58]. For long time of flight, the general TPBVP is expect to be numerically unreasonable to solve. However, since we have constructed

$$\|\mathbf{z}_{\text{desired}} - \mathbf{z}_0\|_2 < \epsilon, \tag{31}$$

for a small $\epsilon > 0$, and continuity of the flow with respect to parameter and spacial variations, we expect that $\|\mathbf{p}_1 - \mathbf{p}_0\|_2$ will likewise be small. In such case, a standard shooting algorithm, based on Newton's method generally works well [29], choosing $\mathbf{p} = \mathbf{p}_0$ as the initial seed. A solution exists for small enough $\epsilon > 0$, and nonsingular Jacobian derivative, by continuation of the trivial solution

$$\mathbf{z}_1 = \mathbf{f}(\mathbf{z}_0, \mathbf{p}_0), \tag{32}$$

along a parameterized solution manifold, $\delta\mathbf{p}(\mathbf{z})$, and $\mathbf{z} = f(\mathbf{z}_0, \mathbf{p}_0 + \delta\mathbf{p}(\mathbf{z}))$, which is an application of the implicit function theorem. In fact, the linearized equations of variation,

$$\dot{\delta\mathbf{z}} = \frac{\partial \mathbf{F}}{\partial \mathbf{z}}(\mathbf{z}, \mathbf{p}) \cdot \delta\mathbf{z} + \frac{\partial \mathbf{F}}{\partial \mathbf{p}}(\mathbf{z}, \mathbf{p}) \cdot \delta\mathbf{p}, \tag{33}$$

can be used to approximately solve for $\mathbf{p}_1$, where $\frac{\partial \mathbf{F}}{\partial \mathbf{z}}$ and $\frac{\partial \mathbf{F}}{\partial \mathbf{p}}$ are respectively the Jacobian matrices of $\mathbf{z}$ and $\mathbf{p}$ variations. We mention that it is possible to model the necessary derivatives using only measured data by appropriately perturbing and observing responses of a physical system [9, 10].

5.2 Time-delayed feedback control

Time-delayed feedback control was first introduced (but not then so-called) by Pyragas [59] who added to Eq. (28) a feedback control perturbation,

$$U(t) = K(x_i(t - T) - x_i(t)), \tag{34}$$

where $x_i(t)$ is one of the component observed variables of $\mathbf{z}(t)$, K is a carefully chosen weighting variable, and the delay T in the control rule was shown to be useful in tuning to the period of a specific UPO; it is easy to see that the amplitude of this control law automatically decreases as the UPO is approached. This method has been generalized and improved by control [60] and "adaptive recognition" [61]. In brief [62], at time t_n, measuring the difference $\delta(t_n)$ between the observed variable $x_i(t_n)$ dynamics, and the goal dynamics $g_i(t_n)$, $\delta(t) = x_i(t_n) - g_i(t_n)$, the local variation rate,

$$\lambda(t_n) = log\left|\frac{\delta(t_n)}{\delta(t_{n-1})}\right|, \tag{35}$$

measures exponential growth rate between actual and desired dynamics. The additive control rule to the observed variable is chosen,

$$U(t_n) = K(t_n)[g_i(t_n) - x_i(t_n)], \tag{36}$$

where,

$$\frac{1}{K(t_n)} = \frac{1}{K_0}(1 - \tanh(\sigma\lambda(t_n))), \sigma > 0, K_0 > 0, \tag{37}$$

This method adapts the strength of the control to the local dynamics, tending to push the actual evolution towards the goal, via a strength adapting to the local instabilities and the error. Notice that choosing $\sigma = 0$ specializes to the Pyragras method. This general set-up allows for the necessary targeting [63] to close the ϵ-chains constructed in previous sections, by choosing the goal dynamics to correspond to successive steps in the designed orbits.

5.3 Dynamic limiting

A particularly simple, and yet extremely effective new technique for stabilizing desired orbits is called "dynamic limiting," by Corron and Pethel [64]. It has been successfully demonstrated experimentally, in a chaotic driven pendulum using a weight, and in a chaotic double scroll circuit using a diode, emphasizing the potential of this passive control strategy [65]. For both experiments, multiple unstable periodic orbits are selectively controlled using minimal perturbations and promises as the authors state that chaos control may apply to a much wider array of important problems.

We describe here dynamic limiting in the following language, using a simple state dependent but otherwise constant addition to the unperturbed dynamical system Eq. (28),

$$\dot{\mathbf{z}} = \mathbf{F}(\mathbf{z}, \mathbf{p}) + \mathbf{G}(\mathbf{z}, t), \tag{38}$$

and,

$$\mathbf{G}(\mathbf{z}, t) = \sum_{n=0}^{\infty}\sum_{i=1}^{N} d_{n,i}\chi_{t_n}(t)\chi_{A_i}(\mathbf{z})\mathbf{k}_i. \tag{39}$$

For each fixed i, $\mathbf{k}_i$ is a constant vector addition to the vectorfield whose influence tends to push trajectories in the general direction of $\mathbf{k}_i$ which should be chosen appropriately pointing towards the goal. Each of the constant vector perturbations $\{\mathbf{k}_i\}_{i=1}^N$ turns on individually due to entering trigger regions of phase space $\{A_i\}_{i=1}^N$, since $\chi_{A_i}(\mathbf{z}) = 1$ if $\mathbf{z} \in A_i, 0$ else, is the usual characteristic function or Heaviside function in the scalar case. Likewise, $\chi_{t_n}(t)$ serves as a switch in time, which turns on if $t_{n-1} < t < t_n$, and if the corresponding decision to do so is on, $d_{n,i} = 1$, as opposed to off, $d_{n,i} = 0$. The degree of pushing depends on the amount of time spent in A_i, and hence accumulated total push, under the influence of the constant perturbation. Notice that this perturbation is only turned-on if the trajectory enters A_i. In practice this is quite simple to implement, in circuit hardware for example as a diode, or in a mechanical system as a weight [65]. For $N > 1$, a panel of diodes allows selection of relative influences. By carefully choosing A_i regions to actuate the influences $\mathbf{k}_i$, for example A_i having a desired periodic orbit on its boundary, relatively complex motions are effectively stabilized in experiment. In fact, in [64], Corron and Pethel used dynamic limiting to control the symbolic dynamics of a Rossler-like attractor LC oscillator.

References

1. Lorenz, E. N. (1963) Deterministic nonperiodic flow. J. Atmos. Sci., **20**:130-141
2. Ott, E., Grebogi, C., Yorke, J. A. (1990) Controlling chaos. Phys. Rev. Lett., **64**:1196–1199
3. Romerias, F., Grebogi, C., Ott, E., Dayawansa, W. (1992) Contolling chaotic dynamical systems. Physica D, **58**(1002):165–192
4. Hirsch, M., Smale, S. (1974) Differential Equations, Dynamical Systems and Linear Algebra. New York: Academic Press
5. Bollt, E., Kostelich, E., (1998) Optimal targeting of chaos. Phys. Lett. A, **245**(5):399–406
6. Shinbrot, T., Ott, E., Grebogi, C., Yorke, J. A. (1992) Using chaos to direct orbits to targets in systems describable by a one-dimensional map. Phys. Rev. A, **45**:4165-4168
7. Shinbrot, T., Grebogi, C., Ott, E., Yorke, J. A. (1993) Using small perturbations to control chaos. Nature, **363**:411–417
8. Bollt, E. (1997) Controlling the chaotic logistic map. PRIMUS (Problems Resources, and Issues in Mathematics Undergraduate Studies), **VII**(1):1–18
9. Shinbrot, T., Ditto, W., Grebogi, C., Ott, E., Spano, M. L., Yorke, J. A. (1992) Using the sensitive dependence of chaos to direct orbits to targets in an experimental chaotic systems. Phys. Rev. Lett., **68**:2863-2866
10. Dolnik, M., Bollt, E. (1998) Communication with chemical chaos in the presence of noise. Chaos, **8**(3):702–710, Bollt, E., Dolnik, M. (1997) Encoding information in chemical chaos by controlling symbolic dynamics. Phys. Rev. E, **55**: 6404-6413
11. Shinbrot, T., Ott, E., Grebogi, C., Yorke, J. A. (1990) Using chaos to direct trajectories to targets. Phys. Rev. Lett., **65**:3215-3218
12. Bollt, E. (1995) Controlling Chaos, Targeting, and Transport. Ph.D thesis, U. Colorado, Boulder

13. Lai, Y. C., Ding, M., Grebogi, C. (1993) Controlling Hamiltonian chaos. Phys. Rev. E, **47**:86-92
14. Bollt, E., Meiss, J. D. (1995) Targeting chaotic orbits to the moon through recurrence. Phys. Lett. A, **204**:373–378
15. Bollt, E., Meiss, J. D. (1995) Controlling chaos through recurrence. Physica D, **81**:280–294
16. Kostelich, E. J., Grebogi, C., Ott, E., Yorke, J. A. (1993) Higher dimensional targeting. Phys. Rev. E, **47**:305-310
17. Barreto, E., Kostelich, E. J., Grebogi, C., Ott, E., Yorke, J. A. (1995) Efficient switching between controlled unstable periodic orbits in higher dimensional chaotic systems. Phys. Rev. E, **51**:4169-4172
18. Kostelich, E. J., Barreto, E. (1997) Targeting and control of chaos. In Control and Chaos, ed. by Judd, K., Mees, A., Teo, K. L., Vincent, T. L. Boston: Birkhäuser, 158–169
19. Kostelich, E., Yorke, J. A. (1987) Lorenz cross sections of the chaotic attractor of the double rotor. Physica D, **24**:263-278
20. Arrowsmith, D. K., Place, C. H. (1990) Introduction to Dynamical Systems. London: Cambridge Univ. Press
21. Meiss, J. D. (1992) Symplectic maps, variational principles, and transport. Reviews of Modern Physics, **64**:795–848
22. Mather, J. N. (1991) Variational construction of orbits of twist diffeomorphisms. J. Am. Math. Soc., **4**:207–263
23. Hanson, J., Cary, J., Meiss, J. (1985) 'Algebraic decay in self-similiar Markov chains. J. Stat. Phys., **39**(3/4):327-345
24. Meiss, J. D., Ott, E. (1987) Markov tree model of transport in area preserving maps. Physica D, **20**:387–402
25. Devaney, R. L. (1989) An Introduction to Chaotic Dynamical Systems. 2nd ed. Redwood City, CA: Addison Wesley
26. Martelli, M., Dong, M., Seph, T. (1998) Defining chaos. Mathematics Magazine, **71**(2):112–122
27. Schroer, C. G., Ott, E. (1997) argeting in Hamiltonian systems that have mixed regular/chaotic phase spaces. Chaos. Focus Issue: Control and Synchronization of Chaos, **7**(4):512–519
28. Szebehely, V. (1967) Theory of Orbits the Restricted Problem of Three Bodies. New York: Academic Press
29. Bollt, E. (2001) Combinatorial control of global dynamics in a chaotic differential equation. Int. J. Bifur. Chaos, **11**(8):2145–2162
30. Rudolph, D. J. (1990) Fundamentals of Measurable Dynamics, Ergodic Theory on Lebesgue Spaces. Oxford: Clarendon Press
31. Bollt, E., Stanford, T., Lai, Y. -C., Zyczkowski, K. (2001) What symbolic dynamics do we get with a misplaced partition? on the validity of threshold crossings analysis of chaotic time-series. Physica D, **154**(3/4):259–286
32. Bollt, E., Stanford, T., Lai, Y. -C., Zyczkowski, K. (2000) Validity of threshold-crossing analysis of symbolic dynamics from chaotic time series. Phys. Rev. Lett. **85**(16):3524–3527
33. Bollt, E. (2003) Review of chaos communication by feedback control of symbolic dynamics. Int. J. Bifur. Chaos, to appear
34. Dolnik, M., Bollt, E. (1998) Communication with chemical chaos in the presence of noise. Chaos, **8**(3):702–710

35. Bollt, E., Lai, Y. -C., Grebogi, C. (1997) Analysis of the topological entropy versus noise resistance trade-off when communicating with chaos. Phys. Rev. Lett., **79**(19):3787–3790
36. Hayes, S., Grebogi, C., Ott, E., Mark, A. (1994) Experimental control of chaos for communication. Phys. Rev. Lett., **73**:1781-1784
37. Hayes, S., Grebogi, C., Ott, E. (1993) Communicating with chaos. Phys. Rev. Lett., **70**:3031-3034
38. Gould, R. (1988) Graph Theory. Menlo Park, CA: Benjamin/Cummings Publishing
39. Bondy, J. A., Murty, U. S. R. (1976), Graph Theory with Applications. New York: American Elsevier
40. de Melo, W., van Strein, S. (1992) One-Dimensional Dynamics. New York: Springer-Verlag
41. Milnor, J., Thurston, W. (1997) On Iterated Maps of the Interval: I and II. Princeton: Princeton Univ. Press
42. Kitchens, B. P. (1998) Symbolic Dynamics, One-sided, Two-sided and Countable State Markov Shifts. New York: Springer-Verlag
43. Lind, D., Marcus, B. (1995) An Introduction to Symbolic Dynamics and Coding. New York: Cambridge Univ. Press
44. Cvitanovic, P. Gunaratne, G., Procaccia, I. (1988) Topological and metric properties of Hénon-type attractors. Phys. Rev. A, **38**:1503–1520
45. Cvitanovic, P. (1991) Periodic orbits as the skeleton of classical and quantum chaos. Physica D, **51**:138-151
46. Cvitanovic, P. (1995) Dynamical averaging in terms of periodic orbits. Physica D, **83**:109–123
47. Grassberger, P., Kantz, H., Moenig, U. (1989) On the symbolic dynamics of the Henon map. J. Phys. A, **22**:5217–5230
48. Smale, S. (1967) Differentiable dynamical systems. Bull AMS, **73**:747-817
49. Bowen, R. (1970) Markov partitions for axiom A diffeomorphisms. Am. J. Math, **92**:725–747
50. Bowen, R. (1975) Equilibrium States and the Ergodic Theory of Anosov Diffeomorphisms. Berlin: Springer-Verlag
51. Bowen, R. (1975) Equilibrium States and the Ergodic Theory of Anosov Diffeomorphisms. Berlin: Springer-Verlag
52. Christiansen, F., Politi, A. (1996) Symbolic encoding in symplectic maps. Nonlinearity, **9**:1623–1640
53. Christiansen F., Politi A. (1997) Guidlines for the construction of a generating partition in the standard map. Physica D, **109**:32–41
54. Hansen, K. (1992) Pruning of orbits in four-disk and hyperbola billiards. Chaos, **2**:71–75
55. Hansen, K. (1993) Symbolic dynamics. I. Finite dispersive billiards. Nonlinearity, **6**:753–769
56. Place, C. M., Arrowsmith ,D. K. (2000) Control of transient chaos in tent maps near crisis. I: Fixed points. Phys. Rev. E, **61**(2):1357–1368; II: Periodic orbits. 1369–1381
57. Neter, J., Kutner, M. H., Nachtsheim, C. J., Wasserman, W. (1996) Applied Linear Regression Models. 3rd ed. Chicago: IRWIN
58. Press, W., Flannery, B., Teukolsky, S., Vetterling, W. (1988) Numerical Recipes in C: The Art of Scientific Computing. New York: Cambridge Univ. Press

59. Pyragas, K. (1992) Continuous control of chaos by self-controlling feedback. Phys. Lett. A, **170**:421–428
60. Boccaletti, S., Arecchi, F. T. (1996) Adaptive recognition and control of chaos. Physica D, **96**:9-16
61. Arecchi, F. T., Bsti, G., Boccaletti, S., Perrone, A. L. (1994) Adaptive recognition of a chaotic dynamics. Europhys. Lett., **26**:327-332
62. Boccalletti, S., Grebogi, C., Lai, Y. -C., Mancini, H., Maza, D. (2000) The control of chaos: theory and applications. Phys. Rep., **329**:103–197
63. Boccalleti, S., Fairini, A., Kostelich, E. J., Arecchi, F. T. (1997) Adaptive targeting of chaos. Phys. Rev. E,. **55**:R4845-R4848
64. Corron, N., Pethel, S. (2002) Control of long periodic orbits and and arbitrary trajectories in chaotic systems using dynamic limiting. **Chaos 12**(1):1–7
65. Corron, N. J., Pethel, S. D., Hopper, B. A. (2000) Controlling chaos with simple limiters. Phy. Rev. Lett., **84**:3835–3838
66. Wiggins, S. (1992) Chaotic Transport in Dynamical Systems. New York: Springer-Verlag
67. Jaeger, L., Kantz, H. (1997) Homoclinic tangencies and non-normal Jacobians – effects of noise in non-hyperbolic systems. Physica D, **105**:79–96